Large-field-of-view laser-scanning OR-PAM using a fibre optic sensor

T. J. Allen, E. Zhang and P.C. Beard

Department of Medical Physics and Biomedical Engineering, University College London, Gower Street, WC1E 6BT, UK

ABSTRACT

Laser-Scanning-Optical-Resolution Photoacoustic Microscopy (LSOR-PAM) requires an ultrasound detector with a low noise equivalent pressure (NEP) and a large angular detection aperture in order to image a large field of view (FOV). It is however challenging to meet these requirements when using piezoelectric receivers since using a small sensing element size (<100μm) in order to achieve a large angular detection aperture will inevitability reduce the sensitivity of the detector as it scales with decreasing element size. Fibre optic ultrasound sensors based on a Fabry Perot cavity do not suffer from this limitation and can provide high detection sensitivity (NEP<0.1kPa over a 20 MHz measurement bandwidth) with a large angular detection aperture due to their small active element size (~10μm). A LSOR-PAM system was developed and combined with this type of fibre optic ultrasound sensor. A set of phantom studies were undertaken. The first study demonstrated that a high resolution image over a large field of view (Ø11mm) could be obtained with a sample-detector separation of only 1.6mm. In the second study, a 12μm diameter tube filled with methylene blue whose absorption coefficient was similar to that of blood was visualised demonstrating that the fibre optic sensor could provide sufficient SNR for in-vivo microvascular OR-PAM imaging. These preliminary results suggest that the fibre optic sensor has the potential to outperform piezoelectric detectors for Laser-Scanning Optical Resolution Photoacoustic Microscopy (LSOR-PAM).

Keywords: Laser-Scanning-Optical-Resolution Photoacoustic Microscopy, LSOR-PAM, Optical-Resolution Photoacoustic Microscopy, ORPAM, Fibre Optics Sensor

1. INTRODUCTION

Optical Resolution Photoacoustic Microscopy (ORPAM) can provide images of superficial microvasculature and other structures with micron scale lateral resolution. Early implementations relied upon mechanically scanning both the focused excitation laser beam and the ultrasound detector over the tissue sample[1]. In order to reduce acquisition time an alternative method has since been reported and is referred to as Laser-Scanning-Optical-Resolution Photoacoustic Microscopy (LSOR-PAM)[2]. This method uses an x–y galvanometer scanner to optically scan the focused excitation beam while detecting the generated photoacoustic signals with a single stationary planar detector offset from the scan area.

LSOR-PAM was first implemented using planar piezoelectric detectors[2,3]. A drawback of these detectors is that, in order to achieve acceptable sensitivity, a relatively large element size (>100μm) is required. However this results in a limited angular detection aperture, requiring the detector to be placed a significant distance (>1cm) from the sample in order to achieve an acceptable field-of-view (>Ø5mm). As a consequence, SNR can be compromised due to acoustic attenuation arising from the geometrical spreading of the wavefront and, to a lesser extent, acoustic absorption. For example, figure 1 (a) shows the directional response of an ideal 400μm diameter circular detector which is comparable to the element sizes previously used for LSOR-PAM[2–5]. The acceptance angle of the detector is ±15 degrees or less for frequencies above 10MHz. Simple geometry dictates that if the detector is orientated at a 45 degree angle and an area of 1cm in diameter is to be imaged (see figure

Photons Plus Ultrasound: Imaging and Sensing 2015, edited by Alexander A. Oraevsky, Lihong V. Wang
Proc. of SPIE Vol. 9323, 93230Z · © 2015 SPIE · CCC code: 1605-7422/15/$18
doi: 10.1117/12.2082815

1(c)), a detector-sample separation of 17mm would be required. Assuming attenuation due to geometrical spreading follows a $1/r^2$ dependence and neglecting acoustic absorption, this will result in the amplitude of the photoacoustic signal being more than an order of magnitude smaller than if the detector-sample separation was 5mm. Indeed, this is perhaps a rather conservative estimate since the acoustic signal frequency content in OR-PAM typically extends well beyond 10 MHz requiring an even larger sample-detector separation if optimum resolution is to be maintained over the entire field-of-view.

In this study, the use of a fibre optic ultrasound detector based on a Fabry Perot sensing cavity is explored as an alternative to piezoelectric detectors previously used in LS-ORPAM. This detector can provide widebandwidth (30MHz), high sensitivity (<0.1kPa NEP) and a wide acceptance angle for frequencies in the tens of MHz range. The measured directivity is shown in figure 1 (b) and shows that the sensor can detect signals as high as 20MHz at angles as large as 90 degrees. This offers the prospect of placing the detector in close proximity to the sample in order to optimise SNR while still being able to achieve a large field-of-view. Micro Ring Resonators (MRR) have also been used as an alternative to piezoelectric detectors for LSOR-PAM[6,7], due to their low NEP (<0.15kPa over a 25 MHz measurement bandwidth) and widebandwidth. However, their reported acceptance angles[7,8] appear to be lower than that of the fibre-optic sensor used in this study.

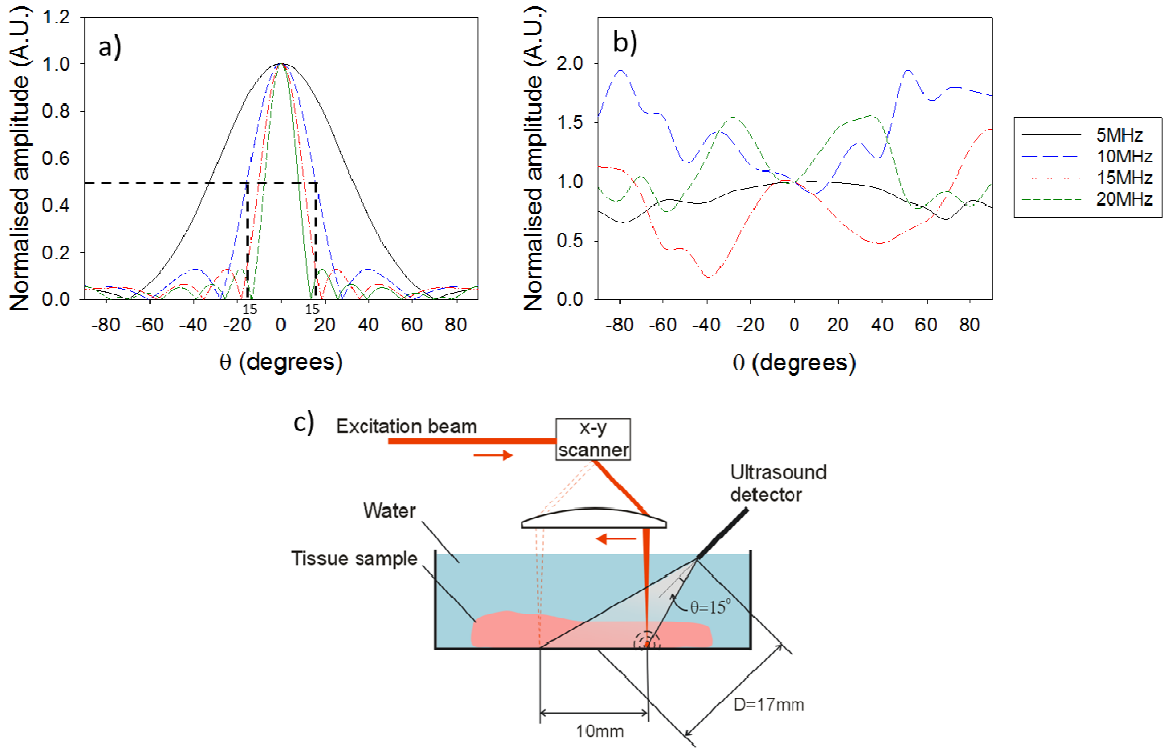

Figure 1 (a) Simulated directivity of an ideal 400µm diameter ultrasound detector obtained using a model of a rigid, circular, pressure detector whose directivity is due purely to spatial averaging. (b) Measured directivity of the fibre optic sensor[9] (c) schematic illustrating that in order to image an area of 10mm in diameter the ideal 400µm diameter detector would need to be placed 17mm away from the sample if the acceptance angle of the detector is 15 degrees

Section 2 describes the LSOR-PAM system and the fibre optic sensor. The lateral resolution of the LSOR-PAM system is described in section 3. Sections 4 and 5 discuss the phantom experiments undertaken. These demonstrate that the system can provide high resolution images over a large field-of-view with the fibre optic sensor in close proximity to the sample and that SNR is sufficient to visualise absorbers with an absorption coefficient similar to that of blood.

2. EXPERIMENTAL SETUP

Figure 2 (a) show the experimental setup. The excitation source consisted of a dye laser pumped by a frequency doubled Q-switched Nd:YAG laser (Elforlight, UK). This provided nanosecond pulses of visible light tunable over the range 560nm to 610nm, a pulse repetition frequency of 5kHz and a pulse energy of 10μJ. The light was coupled into a single mode fibre in order to spatially filter the beam and the divergent output of the fibre was collimated using a lens. The collimated beam was guided via a 2-axis galvanometer scanner through a lens in order to focus the excitation beam on to the sample. The FWHM spot diameter of the beam at the focus was 7μm, the maximum scan area was 14mm × 14mm and the minumum step size was 1μm. Photoacoustic signals were acquired at a rate of a 1000 points per second, limited by the settling time of the galvanometers. The fluence incident on the sample was below 100nJ.

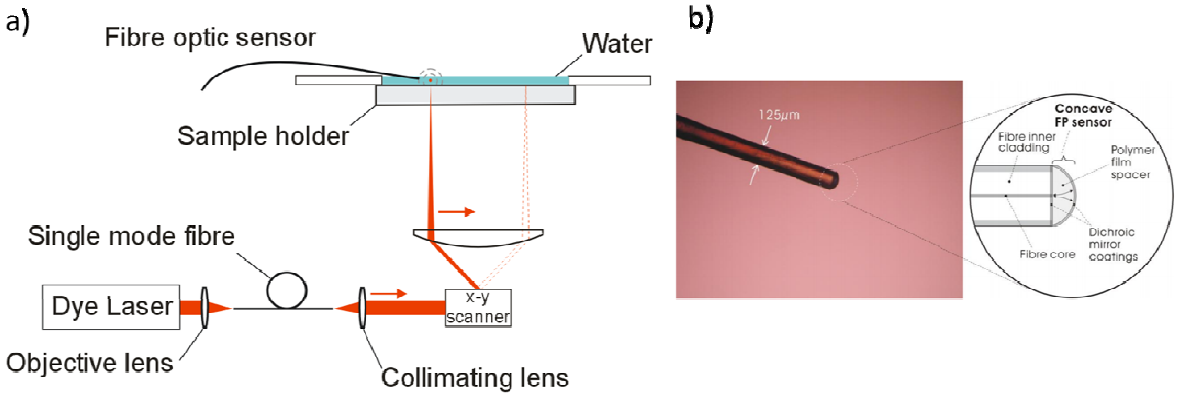

Figure 2 (a) Experimental setup and (b) photograph and schematic of the fibre optic sensor[10]

A photograph and a schematic of the fibre optic sensor are shown in figure 2 (b). The sensor comprised a convex-shaped polymer spacer sandwiched between a pair of dichroic dielectric mirrors deposited on to the tip of a single mode fibre[10]. The core and cladding diameters of the fibre were 10μm and 125μm respectively. The polymer structure acts as an interferometer in which the optical path length is modulated by an incoming acoustic wave thereby modulating its reflectivity. The sensor is interrogated by coupling light into the fibre and detecting the reflected light using a photodiode.

3. CHARACTERISATION OF THE IMAGING SYSTEM

The lateral resolution of the system was quantified by imaging the edge of a black plastic ribbon. Figure 3 (a) shows a photograph of the ribbon and the imaged area is indicated by a dotted box. The photoacoustic image is shown in figure 3 (b) and the imaged area was 60 × 600 μm with step increments of 1μm. An edge spread function (ESF) was obtained from the photoacoustic images (indicated on the photoacoustic image by a dotted line) and plotted in figure 3 (c). Assuming that the beam profile at the focus is Gaussian, a curve was fitted to the measured ESF and its derivative calculated in order to obtain the line spread function (LSF). The FWHM of the LSF was measured to be 7μm providing a measure of the lateral resolution of the system.

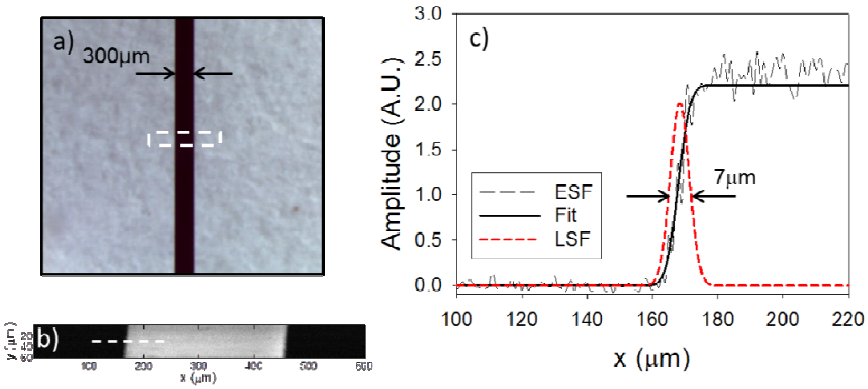

Figure 3: (a) Photograph of the ribbon (the dotted box indicating the area being imaged) (b) Photoacoustic image of the ribbon (c) Edge Spread Function (ESF) obtained from (b) (indicated by the dotted line) and Line spread Function (LSF) calculated by taking the derivative of the ESF.

4. LEAF PHANTOM

To demonstrate that an absorbing target with a complex vessel-like structure can be imaged with high resolution over a large field-of-view, a leaf skeleton dyed with ink was imaged. Figures 5 (a) and (b) show a photograph and a photoacoustic image of the leaf respectively. The imaged area was 8mm by 8mm with step increments of 10µm. The fibre optic sensor was placed at a distance of 1.6mm above the centre of the leaf. This suggests that photoacoustic signals with incident angles up 70 degrees were being detected. A number of carbon fibres (7µm in diameter) were also placed below the leaf phantom (after the photograph was taken) in order to assess if smaller features (<10µm) could be visualised when imaging a large area. The carbon fibres can be identified in the photoacoustic image as indicated by the arrows in figure 5(b). Figures 5 (c) and (d) show respectively a photoacoustic image and a photograph of a smaller region of the leaf indicated by the dotted box on figure 5 (b). The area was 1 × 1mm and the step increment was 1µm. The smaller features of the leaf can clearly be identified in the photoacoustic image and correlate well with those seen in the photograph. The carbon fibres are also clearly visible in the photoacoustic image.

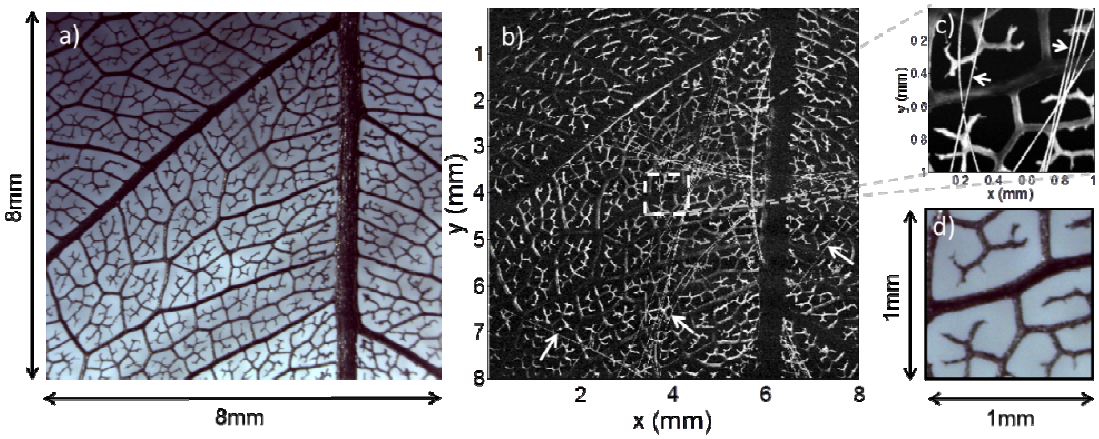

Figure 5: (a) Photograph of the leaf skeleton phantom (b) Photoacoustic image of the leaf skeleton (8 × 8 mm, step size=10µm). (c) High resolution photoacoustic image (1 ×1 mm, step size= 1µm) of the region delineated by the square dotted box in (b) (d) photograph of the region of interest. Carbon fibres were placed below the leaf phantom as indicated by the arrows (the carbon fibres were not in place when the photographs were taken).

5. TISSUE MIMICKING PHANTOM

The leaf skeleton and carbon fibres described in the previous section provide complex micron scale structures that are useful for assessing the potential of the system to provide high resolution images of absorbing anatomical structures such as the microvasculature over a large field of view. However, they are not physiologically realistic in the sense they are likely to be more strongly absorbing than biological chromophores such as haemoglobin. To determine whether the system SNR is sufficient for imaging microvessels (an important OR-PAM application), a more realistic absorber, a 12µm diameter tube (PMMA) filled with methylene blue (μ_a=186cm^{-1} at λ=580nm) and immersed in water was imaged. This absorption coefficient is similar to that of blood at 580nm and the tube diameter is comparable to that of an individual capillary. The imaged area was 300 by 300 µm with step increments of 2 µm. The pulse energy at the focal spot was 100nJ and each detected photoacoustic signal was signal-averaged 4 times. The photoacoustic image obtained is shown in figure 6. This suggests that the system SNR is sufficient to visualise the microvasculature at the level of an individual capillary.

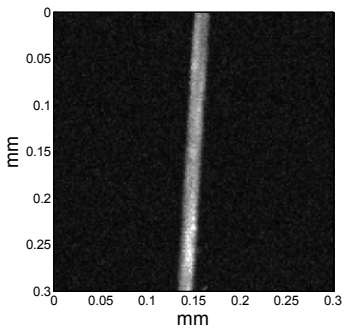

Figure 6: Photoacoustic image of a 12µm diameter tube filled with Methylene blue (μ_a=186cm^{-1} at λ=580nm).

6. CONCLUSION

These preliminary results suggest that the fibre optic sensor used in this study could be a viable alternative to piezoelectric detectors for LSOR-PAM implementations. The large acceptance angle of the sensor allows it to be placed in close proximity to the sample, without compromising the field-of-view. As well as minimising acoustic attenuation this may be advantageous for applications in which a large sample-detector path length is undesirable. Although this study has demonstrated a free-space LSOR-PAM implementation, the small physical size of the fibre optic sensor and its low directional sensitivity suggests it may be useful for endoscopic fibre-optic OR-PAM implementations.

ACKNOWLEDGMENT

The authors acknowledge support from EPSRC and European Union project FAMOS (FP7 ICT, Contract 317744).

REFERENCES

1. Maslov, K., Zhang, H. F., Hu, S. & Wang, L. V Optical-resolution photoacoustic microscopy for in vivo imaging of single capillaries. *Optics Letters* **33**, 929–31 (2008).

2. Xie, Z., Jiao, S., Zhang, H. F. & Puliafito, C. A. Laser-scanning optical-resolution photoacoustic microscopy. *Optics Letters* **34**, 1771–1773 (2009).

3. Zhang, X., Zhang, H. F., Puliafito, C. a. & Jiao, S. Simultaneous in vivo imaging of melanin and lipofuscin in the retina with photoacoustic ophthalmoscopy and autofluorescence imaging. *Journal of Biomedical Optics* **16**, 080504 (2011).

4. Song, W. *et al.* Multimodal photoacoustic ophthalmoscopy in mouse. *Journal of Biophotonics* **6**, 505–12 (2013).

5. Song, W. *et al.* A combined method to quantify the retinal metabolic rate of oxygen using photoacoustic ophthalmoscopy and optical coherence tomography. *Scientific Reports* **4**, 6525 (2014).

6. Xie, Z. *et al.* Pure optical photoacoustic microscopy. *Optics Express* **19**, 9027–34 (2011).

7. Li, H., Dong, B., Zhang, Z., Zhang, H. F. & Sun, C. A transparent broadband ultrasonic detector based on an optical micro-ring resonator for photoacoustic microscopy. *Scientific Reports* **4**, 4496 (2014).

8. Ling, T., Chen, S.-L. & Guo, L. J. High-sensitivity and wide-directivity ultrasound detection using high Q polymer microring resonators. *Applied Physics Letters* **98**, 204103 (2011).

9. Zhang, E. Z. & Beard, P. C. Characteristics of optimized fibre-optic ultrasound receivers for minimally invasive photoacoustic sensing applications. *Proceedings of SPIE* **9323**, 9323–36 (2015).

10. Zhang, E. Z. & Beard, P. C. A miniature all-optical photoacoustic imaging probe. *Proceedings of SPIE* **7899**, 78991F–1– 78991F–6 (2011).